

# On the Stability of Isolated Iridium Sites in N-Rich Frameworks Against Agglomeration Under Reducing Conditions

Andree Iemhoff,<sup>[a]</sup> Maurice Vennwald,<sup>[a]</sup> Jens Artz,<sup>[a]</sup> Chalachew Mebrahtu,<sup>[a]</sup> Alexander Meledin,<sup>[b, c]</sup> Thomas E. Weirich,<sup>[b]</sup> Heinrich Hartmann,<sup>[d]</sup> Astrid Besmehn,<sup>[d]</sup> Matteo Aramini,<sup>[e]</sup> Federica Venturini,<sup>[e]</sup> Fred W. Mosselmanns,<sup>[e]</sup> Georg Held,<sup>[e]</sup> Rosa Arrigo,<sup>[e, f]</sup> and Regina Palkovits<sup>\*[a, g]</sup>

*Dedicated to Professor Holger Braunschweig on the occasion of his 60th birthday.*

Stabilization of single metal atoms is a persistent challenge in heterogeneous catalysis. Especially supported late transition metals are prone to undergo agglomeration to nanoparticles under reducing conditions. In this study, nitrogen-rich covalent triazine frameworks (CTFs) are used to immobilize iridium complexes. Upon reduction at 400 °C, immobilized Ir(acac)(COD) on CTF does not form nanoparticles but transforms into a highly active Ir single atom catalyst. The resulting catalyst systems outperforms both the immobilized complex and supported nanoparticles in the dehydrogenation of formic acid as probe reaction. This superior performance could be traced

back to decisive changes of the coordination geometry positively influencing activity, selectivity and stability. Spectroscopic analysis reveals an increase of electron density on the cationic iridium site by donation from the CTF macroligand after removal of the organic ligand sphere from the Ir(acac)(COD) precursor complex upon reductive treatment. This work demonstrates the ability of nitrogen moieties to stabilize molecular metal species against agglomeration and opens avenues for catalysts design using isolated sites in high-temperature applications under reducing atmosphere.

## Introduction

The quest of isolating metal sites on solid support materials has been one of the major topics in heterogeneous catalysis in the last decade. Great advances in analytical methods in the new century have made it possible to confirm the presence of such sites and their impact on catalytic processes.<sup>[1]</sup> A soaring number of publications has been published in this field, in which innovative synthetic approaches and applications for

these systems are reported together with attempts to unravel the local structure in these intriguing yet challenging systems.<sup>[2]</sup>

Post-synthetic wet impregnation is a common approach for functionalization of heterogeneous supports with isolated metal sites.<sup>[1e,2f,h]</sup> In order to prevent thermodynamically favoured agglomeration of highly dispersed metal sites, suitable anchoring sites on the support are needed.<sup>[2h,3]</sup> Efficient stabilization at high temperatures and oxidative environments has been demonstrated in defect sites or when using reducible oxides.<sup>[2c,3b,4]</sup> However for oxide supports and widely-used late

[a] A. Iemhoff, M. Vennwald, Dr. J. Artz, Dr. C. Mebrahtu, Prof. R. Palkovits  
Chair of Heterogeneous Catalysis and Chemical Technology, ITMC  
RWTH Aachen University  
52074 Aachen (Germany)  
E-mail: palkovits@itmc.rwth-aachen.de

[b] Dr. A. Meledin, Prof. T. E. Weirich  
Central Facility for Electron Microscopy, GFE  
RWTH Aachen University  
52074 Aachen (Germany)

[c] Dr. A. Meledin  
Ernst Ruska-Centre for Microscopy and Spectroscopy with Electrons (ER-C)  
Forschungszentrum Jülich GmbH  
52428 Jülich (Germany)

[d] Dr. H. Hartmann, Dr. A. Besmehn  
Zentralinstitut für Engineering, Elektronik und Analytik ZEA-3  
Forschungszentrum Jülich GmbH  
52425 Jülich (Germany)

[e] Dr. M. Aramini, Dr. F. Venturini, Dr. F. W. Mosselmanns, Prof. G. Held,

Dr. R. Arrigo  
Diamond Light Source  
Harwell Science and Innovation Campus  
Didcot, OX1 10DE (UK)

[f] Dr. R. Arrigo  
School of Science, Engineering and Environment  
University of Salford  
M5 4WT, Manchester (UK)

[g] Prof. R. Palkovits  
Max-Planck-Institute for Chemical Energy Conversion  
45470 Mülheim an der Ruhr (Germany)

 Supporting information for this article is available on the WWW under <https://doi.org/10.1002/cctc.202200179>

 This publication is part of a Special Collection on "Developments in Surface Organometallic and Heterogeneous Single-Atom Catalysts". Please check the ChemCatChem homepage for more articles in the collection.

 © 2022 The Authors. ChemCatChem published by Wiley-VCH GmbH. This is an open access article under the terms of the Creative Commons Attribution Non-Commercial License, which permits use, distribution and reproduction in any medium, provided the original work is properly cited and is not used for commercial purposes.

transition metals, insufficient stabilization is exerted under reducing conditions and particle formation results.<sup>[5]</sup> The benefit of electron-donating oxide materials to hinder agglomeration under reducing conditions has been reported by Kurtog˘lu et al.<sup>[6]</sup> Nitrogen-containing supports such as graphitic carbon nitrides (g-C<sub>3</sub>N<sub>4</sub>) have emerged as an alternative to stabilize isolated, generally positively-charged metal species.<sup>[2f,7]</sup> Palladium single atoms have been reported to be stable up to 150 °C in H<sub>2</sub>, showcasing the potential of nitrogen anchoring sites for stabilization of late transition metals.<sup>[7b]</sup>

Another prominent class of materials containing nitrogen binding sites comprises covalent triazine frameworks (CTFs). Besides widespread ionothermal approaches featuring carbonization of the resulting porous material,<sup>[8]</sup> an innovative polycondensation approach employing (di)-amidines was reported by Wang et al.<sup>[9]</sup> These materials have attracted interest in the field of photocatalysis<sup>[10]</sup> but no attention has been given to applications in heterogeneous catalysis.

The dehydrogenation of formic acid has received attention in the light of the growing interest of storing renewable energy in hydrogen. For this transformation both homogenous<sup>[11]</sup> and heterogeneous catalysts<sup>[12]</sup> have been reported, while through immobilization the high specificity of former systems is met by the advantages in handling and recycling offered by heterogeneous catalysts.<sup>[13]</sup> Upon agglomeration of isolated metal sites and formation of nanoparticles both activity and selectivity are impaired,<sup>[14]</sup> thus providing an indirect characterization of metal speciation of the catalyst upon exposure to reductive conditions.

For the mainly used and scarcely available metal iridium, little is known on the thermal stability of immobilized complexes in nitrogen-rich frameworks. In the case of oxides, the cleavage of organic ligands of immobilized complexes by addition of hydrogen was shown to precede agglomeration towards nanoparticles.<sup>[15]</sup> If suitable anchoring sites are available by the support material, it can act as a stabilizing macroligand for isolated iridium sites as will be demonstrated for the case of CTFs in this contribution.

Active species derived from immobilization of (Acetylacetonato)-(1,5-cyclooctadiene)-iridium(I) (Ir(acac)(COD)) on a polycondensation-based CTF ("CTF-HUST-1") are investigated for the dehydrogenation of formic acid. Influences of a reduction treatment in hydrogen are studied by annular dark field scanning transmission electron microscopy (ADF-STEM) to identify the nuclearity of the Ir species. The electronic structure of the metal sites after reduction is examined by X-ray photoelectron spectroscopy (XPS) and fluorescence-detected X-ray absorption spectroscopy (XAS). Temperature programmed reduction-mass spectrometry (TPR-MS) measurements as well as infrared spectroscopy are used to comment on the changes in ligand sphere from the reductive treatment and the resulting changes in metal support interactions are derived from synchrotron-based in-situ near edge X-ray fine structure (NEXAFS) spectroscopy.

## Results and Discussion

### Catalyst synthesis and characterization

The synthesis of the support material was performed by polycondensation of diamidine and alcohol as reported by Liu et al.<sup>[10a]</sup> The structure of the organic framework was confirmed by infrared and NMR spectroscopy and an ordered structure could be demonstrated by XRD measurements (Figure S1–S3). A specific surface area of 525 m<sup>2</sup>g<sup>-1</sup> with an ill-defined pore structure was derived from nitrogen physisorption experiments (Figure S4). TGA-MS analysis accounts for the stability of the amidine-based material to up to 450 °C, where the decomposition of the framework is accompanied by the formation of HCN (*m/z* = 27) and significant loss of specific surface area (Figure S5 & S6). During optimization of synthesis conditions, 160 °C in the second temperature step was ideal to find a compromise between polymer yield, porosity and sulphur contamination during synthesis in DMSO (Figure S7 & Table S1, see supporting information for further discussion on sulphur contamination from synthesis).

Before further functionalisation, the residual S-content of about 0.6 wt.% was reduced to below 0.2 wt.% by reductive treatment in hydrogen at 300 °C (Figure S12). From N1s XPS measurements, pyridinic nitrogen sites were identified as the main species with minor additional components at higher binding energies (Figure S14).

The immobilization of Ir-complexes on the optimized support material was achieved by wet impregnation in ethanol, adopted from previous studies in our group showing ligand exchange with nitrogen and phosphorus-containing polymers (Figure 1a).<sup>[13b,16]</sup> The impregnation efficiency for a series of iridium complexes is > 95% compared to the targeted metal loading of 1 wt.% Ir and was confirmed by ICP-MS measurements (Table S3). In the catalytic dehydrogenation of formic acid from base-free aqueous solution at 160 °C, the highest TOF of 16900 mol<sub>FA</sub> mol<sub>Ir</sub><sup>-1</sup> h<sup>-1</sup> was obtained when using immobilized Ir(acac)(COD) (Figure S15 & S16). This performance is comparable to literature reports on bipyridine-based COFs<sup>[13b]</sup> and corresponding homogeneous catalysts formed in-situ from the precursor and bipyridine, while outperforming a particulate Ir/C catalyst (Table 1).

ADF-STEM proves the isolated character of the iridium species at atomic resolution in the as synthesized Ir(acac)(COD)/CTF sample (Figure 1b), while a uniform distribution was confirmed using STEM Energy-Dispersive X-ray spectroscopy (STEM-EDX) mapping (Figure S17 & S18). The size of the isolated metal sites (0.1–0.2 nm), appearing as bright contrast features on the dark contrast support material, corresponds well to the atomic diameter of iridium. From infrared spectroscopic measurements on a sample with higher metal loading (9.0 wt.% Ir), the coordination at the nitrogen sites proceeds through the exchange of the COD ligand (L type ligands) (Figure S19). This interaction is reflected in the N1s XPS signal by a decrease in intensity of the signal assigned to pyridinic nitrogen and a corresponding increase of a component at higher binding energy (Figure S20). The Ir4f<sub>7/2</sub> XPS signal is located at 62.0 eV

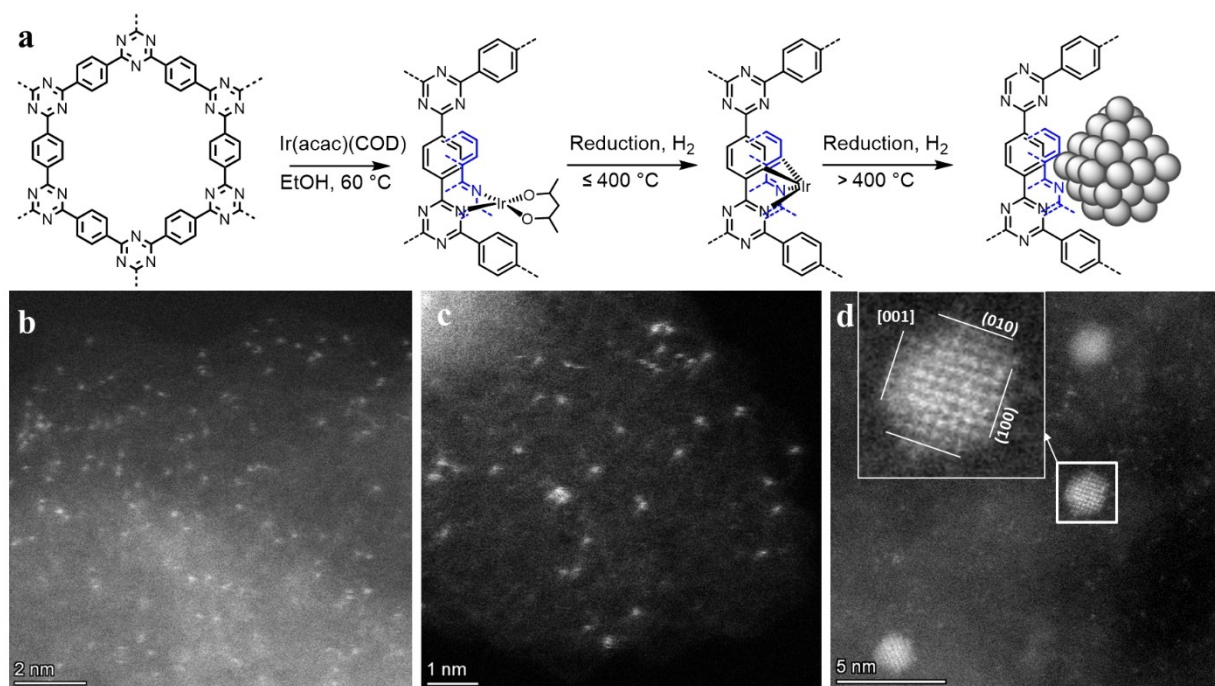


**Figure 1.** (a) Scheme of the functionalization of CTFs with Ir(acac)(COD) and subsequent reduction in hydrogen. Corresponding STEM-images of (b) the sample as functionalized, (c) after reduction at 400 °C and (d) after reduction at 500 °C.

Catalyst	Conversion [%]	TOF [mol <sub>FA</sub> mol <sub>Ir</sub> <sup>-1</sup> h <sup>-1</sup> ]	CO content [ppm]
Ir/C (5 wt.% Ir)	39.9	500 (1500[b])	2045
Ir(acac)(COD)	9.8	1100	n.d.
Ir(acac)(COD)/4,4'-Bipyridine <sup>[a]</sup>	97.0	35800	3020
Ir(ppy) <sub>2</sub> (acac)	98.5	19300	417
Ir(acac)/CTF	98.5	16900	94
Ir(acac)/CTF <sup>c</sup>	99.5	24400	39

Conditions: 6 mL of 10 wt.% FA solution (13.04 mmol FA), 0.022 mol.% of Ir, 160 °C, 750 rpm, 2 h unless plateau pressure value was reached. [a] For in-situ generation of the active complex an excess of 4 eq. bipyridine was used. [b] Turnover frequency calculated based on exposed iridium atoms at the nanoparticle's surface. The dispersion of the catalyst was determined to be 33.4% by CO pulse titration. [c] after reduction at 400 °C.

and shifts to higher binding energies (+0.4 eV) during exposure to air for catalytic tests and reduction treatment, which accounts for oxidation of the initially immobilized Ir(acac)-complex (Figure S21).

### Correlation of dehydrogenation reactivity and iridium nuclearity

During formic acid dehydrogenation, particle formation is a common deactivation pathway with regard to the highly

reductive reaction conditions.<sup>[13b]</sup> Reduction of the catalyst prior to use was performed in order to explore the reactivity of evolving iridium species in dependence of the stabilization by the CTF macroligand. Contrary to expectations of agglomeration upon a reductive treatment, maximum activity and selectivity were obtained after reduction at 400 °C in hydrogen (Table 1 & Figure 2). This translates into an increase of up to 45% in activity and 58% in selectivity compared to the untreated Ir(acac)/CTF. The pronounced difference between the as-synthesized and reduced catalyst can also be seen from recycling experiment, where the former loses 88% of its initial activity after five cycles with an increase of the CO content to more than 700 ppm (Figure 2). For the reduced sample, a significant improvement in stability is observed with still 16800 mol<sub>FA</sub> mol<sub>Ir</sub><sup>-1</sup> h<sup>-1</sup> and a CO content of just 128 ppm after five cycles. ADF-STEM analysis after reduction indicates that the isolated character of the iridium species is maintained up to reduction temperatures of 400 °C (Figure 1c). No particles > 0.5 nm were observed (Figure S22 & S23), while at higher magnification the formation of small clusters (~0.5 nm) as a minor component is visible. The measured size of these entities falls in the range of Ir<sub>4</sub>-clusters, reported by Bayram et al. and Lu et al.<sup>[17]</sup> When the reduction temperature is increased beyond the thermal stability of the support, activity and selectivity deteriorate. This goes along with the carbonization of the CTF framework, which is reflected in an increase in bulk carbon and decrease in nitrogen content from elemental analysis as well as effective iridium loading inducing uncertainties in the calculation of the activity (Table S5 & S6). The damage to the macro-ligand results in agglomeration of the iridium sites, which is

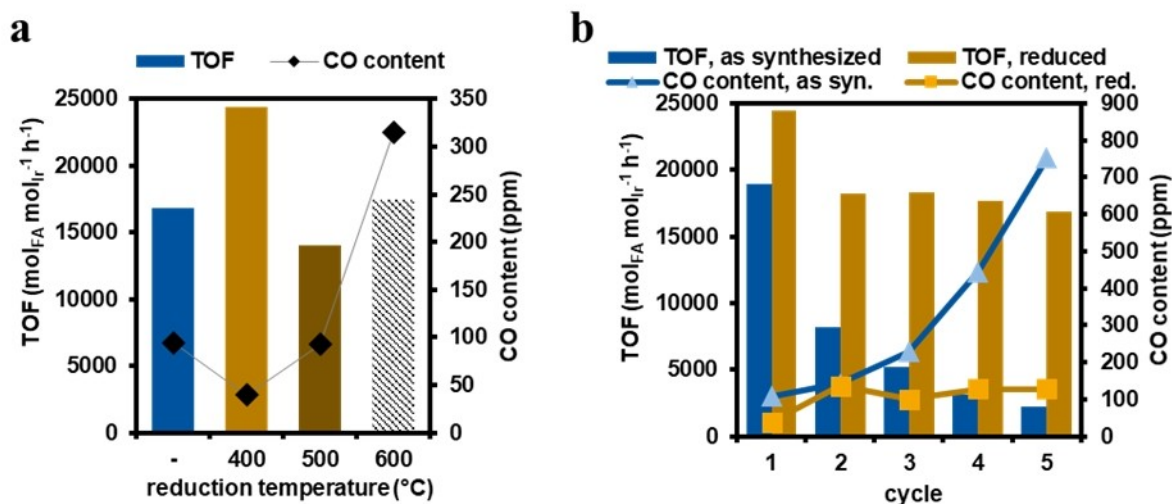


**Figure 2.** Catalytic dehydrogenation of formic acid from aqueous base-free solution using Ir(acac)/CTF. (a) Influence of reduction treatment on activity (TOF) and selectivity (CO content). (b) Stability of Ir(acac)/CTF as synthesized (blue) and after reduction at 400 °C (ochre) in recycling experiments.

reflected in the formation of nanoparticles in the range of 1.5–2.5 nm in TEM images (Figure 1 & Figure S24).

#### Elucidation of metal-support interactions

The interaction of the iridium sites with the CTF after reduction at 400 °C were elucidated using a combination of analytic methods. The fate of the organic ligands during reduction was investigated using TPR-MS at increased iridium loading (9.0 wt.%) and the products of the hydrogenolysis can be observed similar to reports for Ir(acac)<sub>3</sub> impregnated onto silica-based supports (Figure S25).<sup>[18]</sup> This corroborates the initial presence of acac-ligands coordinated to iridium after impregnation. The onset of methane generation as a product of hydrogenolysis of organic ligands occurs at lower temperatures and coincides with the detection of fragments of aliphatic carbons ( $m/z=43$  and  $42$ ) at 250 °C.<sup>[19]</sup> DRIFTS measurements during in-situ reduction reveal that carbon monoxide, which is formed from the hydrogenolysis of the acac ligand (Figure S26), is an intermediary ligand in the reduction process at 300 °C (Figure S28–S30).<sup>[20]</sup>

The electronic structure of the iridium sites was assessed using Ir4f XPS and XAS measurements at the Ir L<sub>III</sub>-edge. A distinct shift in binding energy of the main iridium signal in XPS (Ir 4f<sub>7/2</sub>) to lower binding energies after reduction is observed, indicating a higher electron density at the metal sites (Figure 3a,b). The same trend in energy shift is observed by in-situ reduction in 2 mbar hydrogen using NAP-XPS. Thus, an influence of reoxidation by exposure to air can be ruled out (Figure S31). The assignment of specific oxidation states, as it is routinely done in literature, is ambiguous – especially after reduction –, as different factors such as changes to the ligand sphere, charge transfer with the support and coordination

number can influence the binding energy when dealing with highly dispersed metal species as it was indicated by Vorobyeva et al. and DeRita et al.<sup>[3a,7a]</sup>

The cationic character of the metal sites after reduction can be confirmed by XAS-measurements. From the normalized absorption spectra at the Ir L<sub>III</sub>-edge, the propagation of electrons in 2p<sub>3/2</sub> to partially occupied valence states (5d) is observed, while the intensity depends on its occupation (i.e. oxidation state), symmetry and ligand sphere.<sup>[21]</sup> The intensity of the white line agrees well with Ir(III) in acetylacetonato-bis(2-phenylpyridine)iridium(III) (Ir(ppy)<sub>2</sub>(acac)) (Figure 3c,d). Relative to the as-synthesized sample, the intensity of the white line decreases by a maximum of 0.12% after reduction at 500 °C (cf. Table S7). For this sample, a superposition of particles, identified from ADF-STEM measurements (Figure 1), and isolated metal sites is reflected in the results and illustrates how cationic species are still the dominant one after reduction.

In contrast, the formation of particles as the main species would have resulted in a much more drastic decrease in intensity as observed for particulate Ir/C and Ir-foil (Table S7).<sup>[6,22]</sup> The results agree with those by Kurtoglu et al., where the formation of iridium particles on oxide supports resulted in a decrease of 20% in intensity of white line in XAS, while for the most stable system a decrease of 3% was calculated albeit already for reduction at 100 °C.<sup>[6]</sup>

The Fourier transformed EXAFS spectra reveal changes in the coordination shell of the iridium sites as result of reduction (Figure 4). The main feature at ~1.5 Å narrows significantly after reduction and accounts for a more defined first-shell coordination geometry around the iridium site, which probably had been affected by previous exposure to air. Moreover, a peak at ~2.5 Å appears after reduction.

Based on the good qualitative agreement of this feature with those from Ir(ppy)<sub>2</sub>(acac), a coordination sphere of the

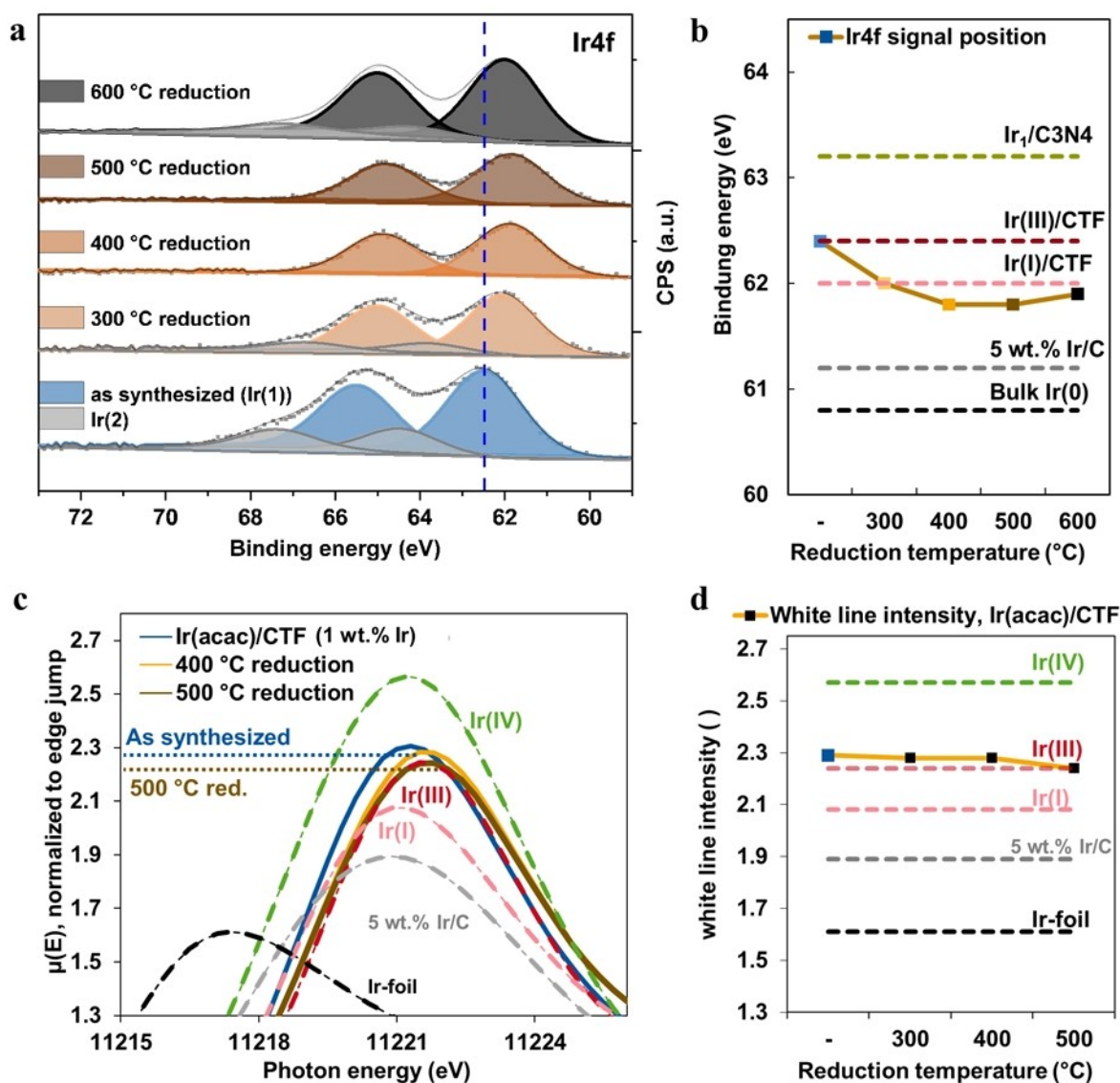


**Figure 3.** Spectroscopic analysis of Ir(acac)/CTF. (a) Ir4f XPS spectra of the catalysts after reduction in hydrogen comprising a main Ir-species, Ir(1), and a secondary species, Ir(2), resulting from exposure of the sample to air prior to the measurement. (b) Shift of the Ir 4f<sub>7/2</sub>-signal in dependence of the reduction temperature in comparison to reference datasets, which were cited from respective publications (Ir<sub>1</sub>/C<sub>3</sub>N<sub>4</sub>,<sup>[1a]</sup> Ir(III)/CTF<sup>[20]</sup> and Ir(0)<sup>[21]</sup>). The shift of Ir(I)/CTF was derived from measurement of Ir(acac)/CTF before exposure to air (Figure S21) and 5 wt.% Ir/C from a reference sample prepared in the course of this work. (c) Normalized XANES-data from x-ray absorption spectroscopy measurements of Ir(acac)/CTF at the Ir L<sub>III</sub>-edge. The full spectrum is shown in Figure S33. (d) The intensity of the white line is plotted against the reduction temperature and compared to standard iridium compounds, which were measured as pure references (see SI for details).

isolated iridium site after reduction at 400 °C can be proposed, apart from Ir–Ir contributions in this region.<sup>[22]</sup> A four-fold coordination with the CTF macroligand is inferred for this sample based on the hydrogenolysis of the organic ligands (Figure 4 & Table 2).

## NEXAFS

The electronic interaction of the nitrogen sites in the CTF support with the iridium sites was elucidated using near edge

X-ray adsorption fine structure (NEXAFS) measurements at the N K-edge (Figure 5). In general, the transition of 1 s electrons (K-edge) to (antibonding) molecular states close to the ionisation energy of the atom is measured. In the nitrogen K-edge spectrum, the main transition at 398.5 eV is assigned to the triazine ring  $\pi^*_{1, C=N-C}$  in accordance with results for s-Triazine,<sup>[23]</sup> Triazine-containing polymers<sup>[24]</sup> and g-C<sub>3</sub>N<sub>4</sub>.<sup>[25]</sup> The high intensity is consistent with the defined molecular structure of the material at hand, especially in comparison to bulk carbon nitrides. Besides, a transition at 399.5 eV is ascribed to additional nitrogen species (e.g. C=N–H) consistent with XPS

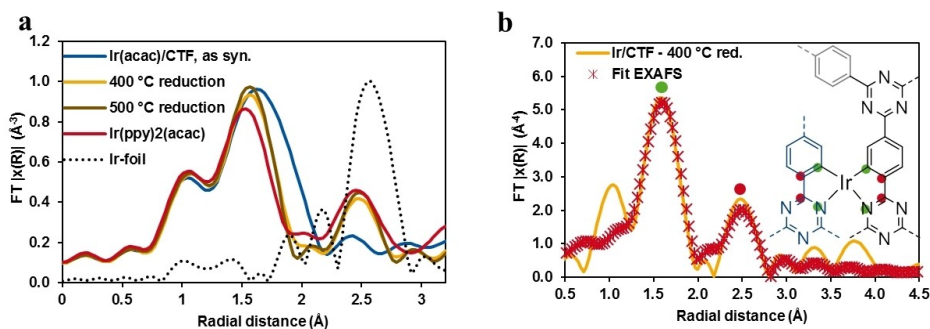


**Figure 4.** Fourier transformed EXAFS data of Ir(acac)/CTF in R-space. (a) Comparison of as synthesized material with samples after reduction as well as Ir(ppy)<sub>2</sub>(acac) and iridium foil. (b) Fit of Ir/CTF data after reduction at 400 °C with a potential structure of the isolated iridium site after reduction.

**Table 2.** Parameters of the Fit of the EXAFS-data in Figure 4(b) of Ir(acac)/CTF after reduction at 400 °C, based on the scattering paths of Ir-(ppy)<sub>2</sub>(acac).

Parameter	Value
Independent points	10.4
Number of variables	6
Fit range	3.00 < k < 11.39
R-factor	0,0296
ΔE <sub>0</sub> (eV)	+8.16
Damping factor, S <sub>0</sub>	1.13 +/- 0.16
Coordination number, N	Ir–N/Ir–C <sub>1</sub> Ir–C <sub>2</sub>
R (Å)	2.0364 ± 0.0129      2.9347 ± 0.0313
σ <sup>2</sup> (Å <sup>2</sup> )	0.00611 ± 0.00202      0.00734 ± 0.0041

analysis, resulting from defect formation during polymerisation or end-capping surface species such as amides and nitriles (Figure S14).<sup>[26]</sup> An overview of the assignment and sources is given in Table S8 in the supporting information. The comparison of the N K-edge NEXAFS of the non-functionalized CTF with Ir(acac)/CTF (1 wt.% Ir) shows that upon functionalization with iridium, broadening of the main  $\pi^*_{1, C=N-C}$  resonance towards higher energy occurs (Figure 5a). Moreover, a decrease

in 1 s- $\sigma^*$  transition intensity at 406.25 eV is observed. This can be interpreted as a  $\sigma$ -style interaction of the nitrogen lone pair with the iridium and charge transfer towards the iridium site, in line with the findings from XPS (Figure S20).<sup>[27]</sup> A large excess of nitrogen in the support material compared to iridium is present with below 0.5% of it as functionalized nitrogen (Ir–N). However, the measurement of two different, chemically equivalent samples (red and blue spectra) confirms that the small changes observed are consistent and relate to the interaction of metal and support.

The in-situ reduction of Ir(acac)/CTF was performed in 0.95 mbar H<sub>2</sub> at 300 and 400 °C, after heating to 200 °C in UHV. In the nitrogen K-edge spectrum, the intensity of the main resonance  $\pi^*_{1, C=N-C}$  increases (Figure 5b). This indicates a higher probability of the N1s- $\pi^*$  transition after reduction, thus a higher number of available states and is consistent with an  $\sigma$ -donation from the nitrogen lone pair to the partially filled iridium d-orbitals.

Because no differences in  $\sigma^*$ -transitions are observed, it can be inferred that the bond distances in the material remain constant during reductive treatment and that the influence is restricted to  $\sigma$ -type coordinative bond between support and metal alone. The increase in the N1s- $\pi^*$  transition upon

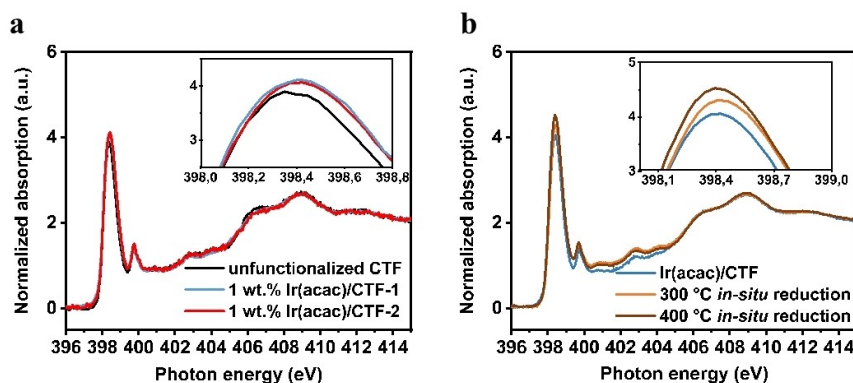


**Figure 5.** NEXAFS analysis of Ir(acac)/CTF (1 wt.% Ir) by measuring TEY. (a) Changes to main  $\pi^*$  resonance as a results of impregnation and reproducibility by comparison of two separate samples in UHV. (b) *In-situ* reduction treatment in hydrogen (0.95 mbar) after measurement in UHV at room temperature.

reduction relative to the as synthesized Ir(acac)/CTF correlates well with the decrease in binding energy of the Ir  $4f_{7/2}$  signal (higher electron density at the iridium sites). A similar increase can be observed in the main  $C1s-\pi^*$  transitions ( $\pi^*_{C=C}$  from phenyl groups), which supports the notion of a Ir–C interaction from the EXAFS model above (Figure S34).

We can postulate that the addition of molecular  $H_2$  to iridium sites further withdraws electron density from the N site. The increase of the intensity of the main  $N1s-\pi^*$  transition for triazine rings ( $\pi^*_{1, C=N-C}$ ) is accompanied by an increase of the intensity of the  $N1s-\pi^*$  transitions at higher binding energies (e.g. as  $C=N-H$ , 403–404 eV), indicating that a partial hydrogenation of the support by the metal site occurs. Nassreddine et al. indicate that iridium might catalyse the hydrogenative decomposition of its ligands in  $Ir(acac)_3$  supported on an amorphous silica-alumina. With regard to the negligible changes to the bulk composition (Table S5), this appears to be a local phenomenon in which the iridium atoms affect their vicinity by hydrogen-spillover.<sup>[18b]</sup>

Subjecting a non-functionalized sample to the same in-situ reduction treatment leads to smaller changes in both carbon and nitrogen K-edge spectra compared to the results for Ir/CTF (Figure S35 & S36) and thus, the effects can be traced back to metal functionalization.

## Conclusion

In this contribution, the application of covalent triazine frameworks (CTFs) for stabilization of isolated iridium sites in harsh reductive conditions is reported. A polycondensation approach allows for the synthesis of an ordered nitrogen-rich support material and iridium centres were introduced by post-synthetic impregnation with  $Ir(acac)(COD)$  via ligand exchange. Despite harsh treatment usually leading to the loss of isolated-well defined sites and formation of particles, the opposite is observed for  $Ir(acac)/CTF$ . Up to a reduction temperature of 400 °C, isolated sites prevail, while beyond this temperature particle formation is observed alongside the decomposition of the support responsible for metal stabilization. This approach differs from the synthesis of single-atom catalysts via copolymerisation at similar temperatures<sup>[1a,28]</sup> in the respect that high temperature treatment is conducted after synthesis. This has the advantage that accessibility of metal sites is not an issue and that changes in the chemical environment of the metal species can be followed and linked to catalytic activity. For  $Ir(acac)/CTF$  improvements in activity, selectivity and stability in the dehydrogenation of formic acid can be traced back to the hydrogenolytic removal of organic ligands, adoption of a different coordination geometry within the framework and increased electron transfer from the CTF macro-ligand to the iridium metal site. It has been demonstrated that, depending on the application, bimolecular metal centres can act as the main reactive sites<sup>[29]</sup> and become preferable to isolated metal sites, which can change their nuclearity under reaction conditions.<sup>[29,30]</sup> In this regard, a deeper understanding of the formed cluster species (~0.5 nm) observed in STEM analysis is

required. Moreover, the convolution of species with different nuclearity is a persistent analytical challenge.<sup>[20]</sup>

Future work will endeavour to unravel specific binding sites in the CTF by virtue of computational methods, as Ir/CTF is situated at the borderline between homogeneous (metal sites comprising organic ligands) and heterogeneous (isolated atoms agglomerating towards clusters and particles) catalysis.

## Experimental Section

General procedures, chemicals used and details on analytical methods can be retrieved from the supporting information file.

**Synthesis of covalent triazine framework:** The synthesis of 1,4-terephthalamidine-dihydrochloride was done according to literature procedures.<sup>[9]</sup> For polycondensation to CTFs, 1,4-terephthalamidine-dihydrochloride (4.05 g, 17.2 mmol, 2 Eq.), 1,4-benzenedimethanol (1.19 g, 8.61 g, 1 Eq.) and  $CsCO_3$  (12.35 g, 37.90 g, 4.4 Eq.) were dispersed in dmso (dry, 300 mL). The dispersion was heated to 100 °C for 24 hours, 160 °C for 36 hours. The dark red solid was filtered from the solution, washed with HCl (aq. 1 M, 3 × 100 mL, colour change to yellow/orange), water (3 × 100 mL), ethanol (3 × 100 mL) and finally THF (3 × 100 mL). The CTF was dried at 80 °C for 48 hours and in vacuo (<0,02 mbar) at 85 °C for 7 hours. A fine yellow powder was obtained (2.47 g, 74.8%). Before functionalization, the material was reduced in a tubular furnace in flowing hydrogen (0.2 L min<sup>-1</sup>) at 300 °C for at least six hours.

**Functionalization with  $Ir(acac)(COD)$ :** Under inert conditions,  $Ir(acac)(COD)$  was dissolved in freshly degassed ethanol and the CTF was added to the solution. The resulting dispersion (~2 g L<sup>-1</sup>) was stirred at 60 °C for 16 hours. The solid was separated from the solution by filtration, dried in vacuo (<0.02 mbar) for 7 hours at 85 °C and stored under argon in a schlenk tube.

**Reduction treatment:**  $Ir(acac)/CTF$  was weighed into a ceramic boat, placed in a tubular furnace and dried at 200 °C in nitrogen flow (0.2 L min<sup>-1</sup>) for one hour. Subsequently, the temperature was increased to the desired reduction temperature at 10 °C/min and the gas was switched to hydrogen (0.2 L min<sup>-1</sup>). The reduction was performed for 3 hours, after which the gas mixture was reverted to nitrogen during cool-down to room temperature. Transfer to and from the oven was done in air.

**Dehydrogenation of formic acid:**  $Ir(acac)/CTF$  (0.022 mol.% Ir, 55.7 mg based on 1 wt.% Ir) was dispersed in aqueous formic acid solution (10 wt.%, 6 mL, 13.03 mmol) with a magnetic stirring bar in an inhouse-designed Hastelloy steel autoclave. The autoclave was sealed and the atmosphere was ex-changed three times with hydrogen to remove residual air. The autoclave was put into a pre-heated aluminium cone at 160 °C and stirred at 750 rpm. The increase of pressure was recorded digitally every 20 seconds. Upon reaching a pressure plateau around 60 bars or after 120 minutes reaction time, the autoclave was transferred into ice. The gas phase was collected and analysed by gas chromatography (Agilent HP6890 GC/TCD, ShinCarbon ST column, He carrier gas). The catalyst was removed from solution by filtration, and the filtrate was analysed by HPLC to confirm full conversion (Shimadzu 2020, organic acid resin column, S-chromatography (Langerwehe), 2 mM trifluoroacetic acid eluent, 40 °C). Leaching of iridium metal into solution was ruled out after analysis of the filtrate by ICP-MS (see Table S4). For recycling experiments, the catalyst was filtered and dried at 80 °C (<0.02 mbar). For the sub-sequent run the amount of aqueous formic acid solution was adjusted relative to the amount of catalyst recovered to maintain a constant ratio of substrate to metal.

The activity (turnover frequency, TOF) was calculated from the increase in pressure by generation of CO<sub>2</sub> and H<sub>2</sub> as reaction products. The rate constant  $k$  (h<sup>-1</sup>) of the associated conversion of formic acid was obtained linear regression of a conversion curve calculated from the pressure time data using Equation (1). A linear increase in pressure over time was observed between 20 and 80% conversion after an initiation period of approx. five minutes during heating-up. Exemplary pressure-time curves are shown in Figure S17.

$$X_{FA} = \frac{p(t)}{p_{final}} = k \cdot t \quad (1)$$

Full conversion from reaching a plateau pressure value was confirmed by HPLC analysis (conversions > 97%).

The selectivity towards CO<sub>2</sub> is expressed as CO content [ppm] in the product gas using Equation (2). A selective reaction (> 99.9% selectivity to CO<sub>2</sub>, e.g. < 1000 ppm CO) was assumed. Response factors of the respective gases were obtained by injection of different volumes of gas mixture of known composition.

$$\text{CO content [ppm]} = \frac{V_{CO}}{V_{CO} + 2V_{CO_2}} \cdot 10^6 \text{ ppm} \quad (2)$$

## Acknowledgements

The authors thank Diamond Light Source for providing beamtime under SP26053 and SI26030. We kindly thank Noah Avraham and Jens Heller for HPLC, XRD and TGA analysis and Meike Emondts for NMR analysis. Sophia Pauschinger, Moritz Haus, Daniel Ditz and Jasmine Idel are thanked for fruitful discussion on the subject. This work was performed as part of the Cluster of Excellence Fuel Science Center (EXC 2186, ID: 390919832) funded by the Excellence Initiative by the German federal and state governments to promote science and research at German universities. All thanks Studienstiftung for support, MV thanks Konrad-Adenauer-Foundation for support. Open Access funding enabled and organized by Projekt DEAL.

## Conflict of Interest

The authors declare no conflict of interest.

## Data Availability Statement

The data that support the findings of this study are available from the corresponding author upon reasonable request.

**Keywords:** covalent triazine framework · formic acid dehydrogenation · heterogeneous catalysis · iridium · metal-support interaction · single-atom catalysis

- [1] a) Z. Chen, S. Mitchell, E. Vorobyeva, R. K. Leary, R. Hauert, T. Furnival, Q. M. Ramasse, J. M. Thomas, P. A. Midgley, D. Dontsova, M. Antonietti, S. Pogodin, N. López, J. Pérez-Ramírez, *Adv. Funct. Mater.* **2017**, *27*; b) S.

- Mitchell, J. Perez-Ramirez, *Nat. Rev. Mater.* **2021**, *6*, 969–985; c) E. D. Boyes, P. L. Gai, *MRS Bull.* **2015**, *40*, 600–609; d) T. E. Martin, R. W. Mitchell, E. D. Boyes, P. L. Gai, *Philos. Trans. R. Soc. A* **2020**, *378*, 20190597; e) M. Soorholtz, L. C. Jones, D. Samuelis, C. Weidenthaler, R. J. White, M.-M. Titirici, D. A. Cullen, T. Zimmermann, M. Antonietti, J. Maier, R. Palkovits, B. F. Chmelka, F. Schüth, *ACS Catal.* **2016**, *6*, 2332–2340; f) T. Zhang, Z. Chen, A. G. Walsh, Y. Li, P. Zhang, *Adv. Mater.* **2020**, *32*, 2002910; g) R. Arrigo, T. Sasaki, J. Callison, D. Gianolio, M. E. Schuster, *J. Energy Chem.* **2021**, *64*, 520–530.
- [2] a) M. Flytzani-Stephanopoulos, B. C. Gates, *Annu. Rev. Chem. Biomol. Eng.* **2012**, *3*, 545–574; b) Y. Chen, Z. Huang, Z. Ma, J. Chen, X. Tang, *Catalysis Science, Technology* **2017**, *7*, 4250–4258; c) R. Lang, W. Xi, J. C. Liu, Y. T. Cui, T. Li, A. F. Lee, F. Chen, Y. Chen, L. Li, L. Li, S. Miao, X. Liu, A. Q. Wang, X. Wang, J. Luo, B. Qiao, J. Li, T. Zhang, *Nat. Commun.* **2019**, *10*, 234; d) W. Liu, L. Zhang, X. Liu, X. Liu, X. Yang, S. Miao, W. Wang, A. Wang, T. Zhang, *J. Am. Chem. Soc.* **2017**, *139*, 10790–10798; e) Y. Ren, Y. Tang, L. Zhang, X. Liu, L. Li, S. Miao, D. Sheng Su, A. Wang, J. Li, T. Zhang, *Nat. Commun.* **2019**, *10*, 4500; f) G. Vile, D. Albani, M. Nachtegaal, Z. Chen, D. Dontsova, M. Antonietti, N. Lopez, J. Perez-Ramirez, *Angew. Chem. Int. Ed. Engl.* **2015**, *54*, 11265–11269; g) E. Vorobyeva, E. Fako, Z. Chen, S. M. Collins, D. Johnstone, P. A. Midgley, R. Hauert, O. V. Safonova, G. Vile, N. Lopez, S. Mitchell, J. Pérez-Ramírez, *Angew. Chem. Int. Ed. Engl.* **2019**, *58*, 8724–8729; h) B. Qiao, A. Wang, X. Yang, L. F. Allard, Z. Jiang, Y. Cui, J. Liu, J. Li, T. Zhang, *Nat. Chem.* **2011**, *3*, 634.
- [3] a) L. DeRita, J. Resasco, S. Dai, A. Boubnov, H. V. Thang, A. S. Hoffman, I. Ro, G. W. Graham, S. R. Bare, G. Pacchioni, X. Pan, P. Christopher, *Nat. Mater.* **2019**, *18*, 746–751; b) J. Jones, H. Xiong, A. T. DeLaRiva, E. J. Peterson, H. Pham, S. R. Challa, G. Qi, S. Oh, M. H. Wiebenga, X. I. Pereira Hernández, Y. Wang, A. K. Datye, *Science* **2016**, *353*, 150–154.
- [4] M. Moliner, J. E. Gabay, C. E. Kliewer, R. T. Carr, J. Guzman, G. L. Casty, P. Serna, A. Corma, *J. Am. Chem. Soc.* **2016**, *138*, 15743–15750.
- [5] a) F. Héroguel, D. Gebert, M. D. Detwiler, D. Y. Zemlyanov, D. Baudouin, C. Copéret, *J. Catal.* **2014**, *316*, 260–269; b) C. Coperet, *Acc. Chem. Res.* **2019**, *52*, 1697–1708.
- [6] S. F. Kurtoğlu, A. S. Hoffman, D. Akgül, M. Babucci, V. Aviyente, B. C. Gates, S. R. Bare, A. Uzun, *ACS Catal.* **2020**, *10*, 12354–12358.
- [7] a) E. Vorobyeva, Z. Chen, S. Mitchell, R. K. Leary, P. Midgley, J. M. Thomas, R. Hauert, E. Fako, N. López, J. Pérez-Ramírez, *J. Mater. Chem. A* **2017**, *5*, 16393–16403; b) Z. Chen, E. Vorobyeva, S. Mitchell, E. Fako, N. López, S. M. Collins, R. K. Leary, P. A. Midgley, R. Hauert, J. Pérez-Ramírez, *Nat. Sci. Rev.* **2018**, *5*, 642–652.
- [8] a) D. Y. Osadchii, A. I. Olivos-Suarez, A. V. Bavykina, J. Gascon, *Langmuir* **2017**, *33*, 14278–14285; b) A. Iemhoff, J. Deischter, S. Jung, G. Tuci, G. Giambastiani, R. Palkovits, *J. Mater. Chem. A* **2021**, *9*, 5390–5403.
- [9] K. Wang, L.-M. Yang, X. Wang, L. Guo, G. Cheng, C. Zhang, S. Jin, B. Tan, A. Cooper, *Angew. Chem. Int. Ed.* **2017**, *56*, 14149–14153; *Angew. Chem.* **2017**, *129*, 14337–14341.
- [10] a) M. Liu, Q. Huang, S. Wang, Z. Li, B. Li, B. Tan, S. Jin, *Angew. Chem. Int. Ed. Engl.* **2018**; b) M. Liu, X. Wang, J. Liu, K. Wang, S. Jin, B. Tan, *ACS Appl. Mater. Interfaces* **2020**, *12*, 12774–12782.
- [11] a) J. F. Hull, Y. Himeda, W.-H. Wang, B. Hashiguchi, R. Periana, D. J. Szalda, J. T. Muckerman, E. Fujita, *Nat. Chem.* **2012**, *4*, 383–388; b) S. Kar, M. Rauch, G. Leitus, Y. Ben-David, D. Milstein, *Nature Catalysis* **2021**, *4*, 193–201.
- [12] a) K. Tedsree, T. Li, S. Jones, C. W. Chan, K. M. Yu, P. A. Bagot, E. A. Marquis, G. D. Smith, S. C. Tsang, *Nat. Nanotechnol.* **2011**, *6*, 302–307; b) Q. Y. Bi, J. D. Lin, Y. M. Liu, H. Y. He, F. Q. Huang, Y. Cao, *Angew. Chem. Int. Ed. Engl.* **2016**, *55*, 11849–11853.
- [13] a) A. V. Bavykina, M. G. Goesten, F. Kapteijn, M. Makkee, J. Gascon, *ChemSusChem* **2015**, *8*, 809–812; b) C. Broicher, S. R. Foit, M. Rose, P. J. C. Hausoul, R. Palkovits, *ACS Catal.* **2017**, *7*, 8413–8419.
- [14] F. Solymosi, Á. Koós, N. Liliom, I. Ugrai, *J. Catal.* **2011**, *279*, 213–219.
- [15] J. Lu, C. Aydin, N. D. Browning, B. C. Gates, *J. Am. Chem. Soc.* **2012**, *134*, 5022–5025.
- [16] P. J. C. Hausoul, C. Broicher, R. Vegliante, C. Göb, R. Palkovits, *Angew. Chem. Int. Ed.* **2016**, *55*, 5597–5601; *Angew. Chem.* **2016**, *128*, 5687–5691.
- [17] a) E. Bayram, J. Lu, C. Aydin, N. D. Browning, S. Özkaz, E. Finney, B. C. Gates, R. G. Finke, *ACS Catal.* **2015**, *5*, 3514–3527; b) J. Lu, P. Serna, C. Aydin, N. D. Browning, B. C. Gates, *J. Am. Chem. Soc.* **2011**, *133*, 16186–16195.
- [18] a) F. Héroguel, G. Siddiqi, M. D. Detwiler, D. Y. Zemlyanov, O. V. Safonova, C. Copéret, *J. Catal.* **2015**, *321*, 81–89; b) S. Nassreddine, G.

- Bergeret, B. Jouguet, C. Geantet, L. Piccolo, *Phys. Chem. Chem. Phys.* **2010**, *12*, 7812–7820.
- [19] a) W. E. Wallace, *Butane in Mass Spectra by NIST Mass Spectrometry Data Center*, National Institute of Standards and Technology, Gaithersburg, MD, **2014**; b) W. E. Wallace, *Pentane in Mass Spectra by NIST Mass Spectrometry Data Center*, National Institute of Standards and Technology, Gaithersburg, MD, **2014**.
- [20] Y. Lu, C.-T. Kuo, L. Kovarik, A. S. Hoffman, A. Boubnov, D. M. Driscoll, J. R. Morris, S. R. Bare, A. M. Karim, *J. Catal.* **2019**, *378*, 121–130.
- [21] F. M. F. de Groot, A. Knop-Gericke, T. Ressler, J. A. Van Bokhoven, in *In-situ Spectroscopy of Catalysts* (Ed.: B. M. Weckhuysen), American Scientific Publishers, Utrecht, **2004**.
- [22] X. Shao, X. Yang, J. Xu, S. Liu, S. Miao, X. Liu, X. Su, H. Duan, Y. Huang, T. Zhang, *Chem* **2019**, *5*, 693–705.
- [23] E. Apen, A. P. Hitchcock, J. L. Gland, *J. Phys. Chem.* **1993**, *97*, 6859–6866.
- [24] A. Fujimori, N. Sato, K. Kanai, Y. Ouchi, K. Seki, *Langmuir* **2009**, *25*, 1112–1121.
- [25] I. Y. Kim, S. Kim, X. Jin, S. Premkumar, G. Chandra, N.-S. Lee, G. P. Mane, S.-J. Hwang, S. Umaphathy, A. Vinu, *Angew. Chem. Int. Ed.* **2018**, *57*, 17135–17140; *Angew. Chem.* **2018**, *130*, 17381–17386.
- [26] P. S. Johnson, P. L. Cook, X. Liu, W. Yang, Y. Bai, N. L. Abbott, F. J. Himpsel, *J. Chem. Phys.* **2011**, *135*, 044702.
- [27] a) R. Arrigo, M. E. Schuster, Z. Xie, Y. Yi, G. Wowsnick, L. L. Sun, K. E. Hermann, M. Friedrich, P. Kast, M. Hävecker, A. Knop-Gericke, R. Schlögl, *ACS Catal.* **2015**, *5*, 2740–2753; b) J. M. García-Lastra, P. L. Cook, F. J. Himpsel, A. Rubio, *J. Chem. Phys.* **2010**, *133*, 151103; c) C. Battocchio, I. Fratoddi, G. Iucci, M. V. Russo, A. Goldoni, P. Parent, G. Polzonetti, *Mater. Sci. Eng. C* **2007**, *27*, 1338–1342; d) C. D. Pemmaraju, R. Copping, S. Wang, M. Janousch, S. J. Teat, T. Tyliczak, A. Canning, D. K. Shuh, D. Prendergast, *Inorg. Chem.* **2014**, *53*, 11415–11425; e) W. E. Kaden, T. Wu, W. A. Kunkel, S. L. Anderson, *Science* **2009**, *326*, 826; f) L. Zhang, R. Long, Y. Zhang, D. Duan, Y. Xiong, Y. Zhang, Y. Bi, *Angew. Chem. Int. Ed. Engl.* **2020**, *59*, 6224–6229.
- [28] G. Vilé, G. Di Liberto, S. Tosoni, A. Sivo, V. Ruta, M. Nachttegaal, A. H. Clark, S. Agnoli, Y. Zou, A. Savateev, M. Antonietti, G. Pacchioni, *ACS Catal.* **2022**, *12*, 2947–2958.
- [29] C. P. Gordon, H. Engler, A. S. Tragl, M. Plodinec, T. Lunkenbein, A. Berkessel, J. H. Teles, A.-N. Parvulescu, C. Copéret, *Nature* **2020**, *586*, 708–713.
- [30] L. Liu, D. M. Meira, R. Arenal, P. Concepcion, A. V. Puga, A. Corma, *ACS Catal.* **2019**, *9*, 10626–10639.

---

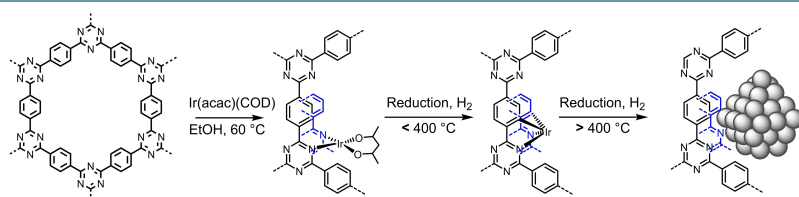
Manuscript received: February 3, 2022

Revised manuscript received: March 23, 2022

Accepted manuscript online: March 29, 2022

Version of record online: ■■■, ■■■■

## RESEARCH ARTICLE



**Formic acid dehydrogenation:** Upon reduction at 400 °C, immobilized Ir-(acac)(COD) on CTF transforms into a highly active Ir single atom catalyst. The resulting catalyst systems outperform both the immobilized complex and supported nanoparticles in the

dehydrogenation of formic acid as model reaction. This superior performance could be traced back to decisive changes of the coordination geometry and increased electron transfer from the CTF macro-ligand to the iridium metal site.

*A. Iemhoff, M. Vennewald, Dr. J. Artz, Dr. C. Mebrahtu, Dr. A. Meledin, Prof. T. E. Weirich, Dr. H. Hartmann, Dr. A. Besmehn, Dr. M. Aramini, Dr. F. Venturini, Dr. F. W. Mosselmans, Prof. G. Held, Dr. R. Arrigo, Prof. R. Palkovits\**

1 – 10

**On the Stability of Isolated Iridium Sites in N-Rich Frameworks Against Agglomeration Under Reducing Conditions**



Special Collection